ACS OMEGA

Article

Cite This: ACS Omega 2018, 3, 15606−15614

http://pubs.acs.org/journal/acsodf

Naringin−Chalcone Bioflavonoid-Protected Nanocolloids: Mode of Flavonoid Adsorption, a Determinant for Protein Extraction

Divya Mandial,[§] Poonam Khullar,*[,§] Harsh Kumar,[∥] Gurinder Kaur Ahluwalia,[‡] and Mandeep Singh Bakshi*[,†]

[†]Department of Natural and Applied Sciences, University of Wisconsin−Green Bay, 2420 Nicolet Drive, Green Bay, Wisconsin 54311-7001, United States

[‡]Nanotechnology Research Laboratory, College of North Atlantic, Labrador City, Newfoundland and Labrador A2V 2K7, Canada

[§]Department of Chemistry, B.B.K. D.A.V. College for Women, Amritsar 143005 Punjab, India

[∥]Department of Chemistry, Dr. B. R. Ambedkar National Institute of Technology, Jalandhar, 144011 Punjab, India

Supporting Information

ABSTRACT: In order to highlight the applications of bioflavonoids in materials chemistry, naringin and its chalcone form were used in the nanomaterial synthesis to produce flavonoid-conjugated nanomaterials in aqueous phase. Chalcone form proved to be excellent reducing as well as stabilizing agent in the synthesis of monodisperse Au, Ag, and Pd nanoparticles (NPs) of ∼5−15 nm, following in situ reaction conditions where no external reducing or stabilizing agents were used. The mechanism of NP surface adsorption of flavonoid was determined with the help of dynamic light scattering and zeta potential measurements. Surface-adsorbed flavonoids also allowed NPs to easily transfer into the organic phase by using aqueous insoluble ionic liquid. Pd NPs attracted the excessive amount of surface adsorption of both naringin as well as its chalcone form that in turn drove Pd NPs in self-assembled state in comparison to Au or Ag NPs. An amount of surface-adsorbed flavonoids selectively determined the extraction of protein fractions from complex zein corn starch protein solution. Self-assembled Pd NPs with a large amount of surface-adsorbed naringin preferentially extracted zein fraction of higher molar mass, whereas Au and Ag NPs almost equally extracted the zein fractions of lower molar masses.

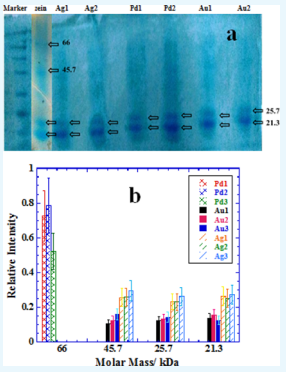

INTRODUCTION

Bitter taste of the grapefruit juice stems from a very important flavonoid naringin, a polyphenolic natural product, that metabolizes to naringenin in the human physiological system with extraordinary health benefits such as antioxidant, anticancer, and antihepatitis C virus production and is a useful ingredient in the formulations of cardio-vascular treatments.[1−3] This unique flavonoid still remains elusive for its applications in the synthesis of nanomaterials with possible implications in food and pharmaceutical industries.[4−6] Naringin is water-soluble and can be easily used in aqueous-based green synthesis of different nanomaterials. The most important and significant property of naringin is its transformation into corresponding chalcone (Figure 1), a semisynthetic sweetener in the basic medium with considerable commercial potential.[7−9] This is well documented in several previous studies[10,11] and very much depends on the pH. An appropriate treatment of chalcone solution with HCl and NaCl allows it to extract in semisolid or powder form of light yellow color. In this study, we demonstrate the potential of both naringin as well as chalcone in the synthesis of different nanomaterials, which stems from the metal-chelating[12,13] ability of flavonoids with transition metal ions through strong complexation. Several studies have been devoted in this direction, where these complexes act as strong antioxidants and anti-free radical agents.[14,15] Usually, the most abundant metal complexes are composed of one deprotonated flavonoid molecule, transition metal ion, and an additional neutral flavonoid molecule. Chelate complexes are mainly square planar as in the case of Cu^{II} with coordination from hydroxyl group of carbon 5 and carbonyl moiety at carbon 4 on the ring 2 (Figure 1).[12,13] However, multiple coordination sites are also expected depending on the oxidation state of the metal ion.

As coordination reduces the electron density on flavonoid, flavonoid acts as a good reducing agent to convert metal ions into corresponding nanoparticles (NPs). We have explored and compared this ability of naringin and its chalcone in the synthesis of Au, Ag, and Pd NPs in different media to demonstrate their respective potential for different nanomaterials synthesis, their surface adsorption behavior, and applications of flavonoid-conjugated nanomaterials for protein extraction. Electron donating behavior of naringin promotes its excellent complexing and flocculating abilities to extract nanomaterials from the aqueous suspensions. Flavonoid−protein interactions[16−18] is another important subject in view of designing new naringin-inspired drugs. This can be very well

Received: July 25, 2018
Accepted: October 29, 2018
Published: November 16, 2018

DOI: 10.1021/acsomega.8b01776
ACS Omega 2018, 3, 15606−15614

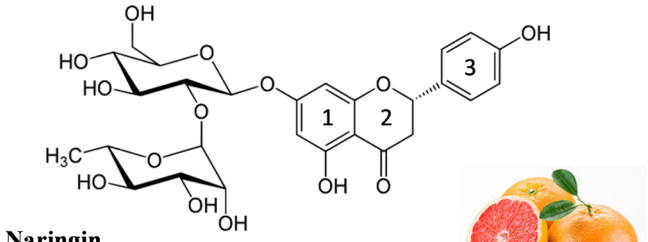

Naringin

7-[[2-*O*-(6-Deoxy-α-L-mannopyranosyl)-β-D-glucopyranosyl]oxy]-2,3-dihydro-5-hydroxy-2-(4-hydroxyphenyl)-4*H*-1-benzopyran-4-one ((7–rhamnoglucosyl-4,5-dihydroxyflavanone))

Bioflavonoids

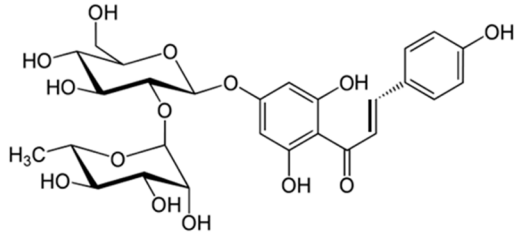

Chalcone

(4–rhamnoglucosyl-2,6,4 trihydroxychalcone)

Figure 1. Molecular structures of naringin and its chalcone form.

exploited by using flavonoid-conjugated nanomaterials in selective extraction of proteins from complex biological mixtures with possible ramifications in biotechnology. We demonstrate this by using naringin-conjugated NPs for the extractions of protein fractions from aqueous solutions of zein protein which is an important component of corn starch protein and possesses numerous applications in the food industry. Thus, the aim of present study is to explore and highlight the fundamental materials chemistry[19,20] aspects of both naringin and its chalcone in synthesizing flavonoid-conjugated nanomaterials with possible implications in food and pharmaceutical industries.

RESULTS AND DISCUSSION

Photophysical Properties of Naringin. Aqueous solution of naringin exhibits a remarkable color change when its pH is changed from neutral to basic by using NaOH because of its gradual conversion into chalcone (Figure 2a). Highly dilute solution of naringin (<1 mM) provides most of the peaks in the UV region due to $\pi \rightarrow \pi^*$ transitions of ring 1,[21] however, higher concentration (ca. 50 mM) produces a main prominent peak around 390 nm (Figure 2a) that red-shifts into the visible region as pH increases. This provides a bright yellow-orange color (see the color change in cuvettes) because of the ionization of the phenolic groups of flavonoid.[19] The mechanism for the flavanone–chalcone isomerization equilibrium of naringin in basic medium is carried out through the carbanion intermediate[21] and brings a large increase in the intensity and wavelength shift (~110 nm) over a pH range from 7 to 12 as depicted in the inset of Figure 2a. The corresponding fluorescence emission spectrum of aqueous naringin shows strong emission around 490 nm when excited at 390 nm (Figure 2b). A remarkable quenching of this emission band with significant red shift occurs as the pH of the medium increases. Both fluorescence intensity and wavelength shift have been plotted in the inset, where actual flavanone–

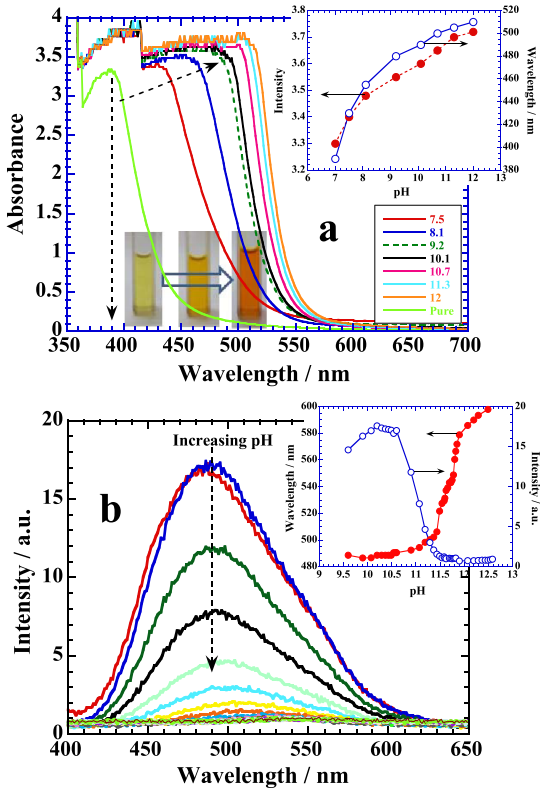

Figure 2. (a) UV–visible titration of naringin with NaOH. Inset: Color change with the change in pH of the solution from 7 to 12. Plot of intensity and wavelength change with pH. (b) Plots of fluorescence emission of the same titration with pH. Inset: Variation in the emission intensity and wavelength with pH. See details in the text.

chalcone isomerization occurs around pH 11.2. Interestingly, addition of HCl to naringin solution reduces the pH but does not affect the absorption spectrum (Supporting Information, Figure S1) because it only induces the protonation of naringin.

Flavanone–Chalcone-Mediated Synthesis of Au NPs. Flavanone–chalcone isomerization under the effect of pH variation demonstrates dramatic effects on the synthesis of Au NPs. At low pH, few settled Au NPs are produced (Figure 3a, see bottle "E"), and the in situ reduction reaction is not significant because the protonated form of naringin is unable to effectively reduce Au(III) into Au(0), and hence, no colloidal suspension is produced. However, the reaction facilitates at neutral pH (bottle "B") with a better yield but NPs got aggregated and no colloidal suspension is obtained. The reaction is highly facilitated in the basic medium (bottle "F"), where the chalcone form proves to be an excellent reducing as well as stabilizing agent in comparison to naringin because of the open ring 2 (Figure 1) that provides better fluxional ability for the chelation. It results in a fine colloidal suspension.[22] Interestingly, if we decant the upper clear solutions of bottles "E" and "B" that contain excess of aqueous naringin, then purify NPs with pure water, collect them, and add 0.1 M aqueous NaOH, we get a bright orange colloidal suspension of NPs simply by agitating the solution because of the formation of chalcone (see cuvette "C") that gives strong characteristic absorbance band of chalcone around 480 nm in basic medium (as noted previously in Figure 2a) and a very weak broad hump because of the surface plasmon resonance (SPR) of Au NPs around 680 nm[19] (Figure 3b, indicated by a block arrow). In contrast, if we dissolve the settled Au NPs of bottle "B" in

DOI: 10.1021/acsomega.8b01776
ACS Omega 2018, 3, 15606–15614

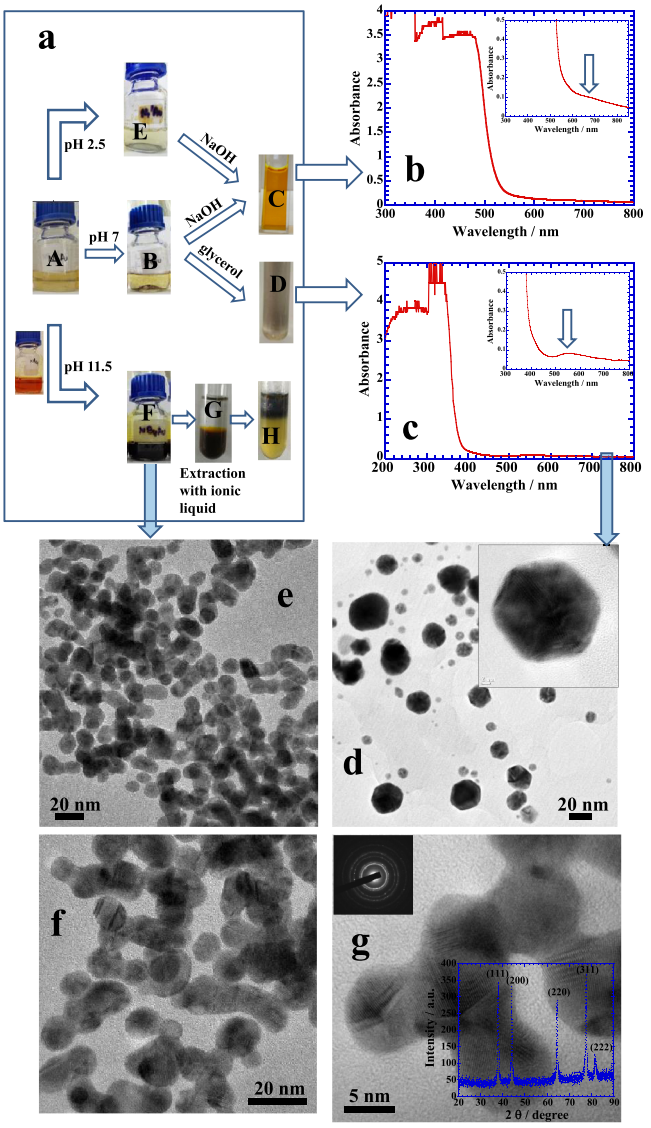

Figure 3. (a) Reaction sequences of in situ reaction of naringin with 0.25 mM of aqueous $HAuCl_4$, at pH = 2.5, 7, and 11.5. Bottles "E", "B", and "F" show the Au NP solutions prepared, respectively. Au NPs of bottle "E" and "B" can be made stable suspensions with basic medium and glycerol, respectively, while that of "F" can be extracted into the organic phase. (b,c) UV−visible scans of the respective samples. TEM images of Au NPs (d) prepared with naringin and (e−g) prepared with its chalcone. Inset of (g) depicts the XRD patterns of Au NPs. See details in text.

glycerol rather than aqueous NaOH, we get a dark colloidal suspension (cuvette D) with no absorbance of chalcone around 480 nm. Rather a combination of characteristic band of naringin appears between 300 and 400 nm in its neutral form (Figure 3c) and a much stronger absorbance of Au NPs at shorter wavelength around 560 nm is produced. A large difference in the absorbance of Au NPs in Figure 3b (at 680 nm) and in Figure 3c (at 560 nm) is simply due to an extent of self-aggregation in the two different colloidal solutions, that is, in the basic medium and glycerol, respectively. Thus, Au NPs produced at pH 2.5 and 7 under in situ reaction conditions of naringin can be made colloidal suspensions in basic medium and/or in glycerol in neutral medium, whereas Au NPs produced at pH 11.5 (bottle "F") can be easily extracted in the organic phase by using water-insoluble ionic liquids (ILs) such as 1-butyl-3-methylimidazolium hexafluorophosphate (see sequence "F → G → H").[23]

Transmission electron microscopy (TEM) images of Au NPs synthesized by using naringin (at pH 7) and chalcone (at pH 11.5) are shown in Figure 3d−g, respectively. Chalcone is considered to be a much better reducing and shape controlling agent to produce relatively smaller spherical NPs less than 10 nm though they mostly exist in the merged state with one another in comparison to naringin. Naringin produces NPs of variable sizes (7−40 nm) and shapes along with long needles of self-crystallized naringin (Figure S2). Naringin is known for its self-crystallization under different experimental conditions.[6,24−26] Several factors lead to the crystallization of naringin and among them presence of salts or different solubility criteria are the main forces that drive naringin molecules for self-crystallization.

Morphology-controlled growth of a crystal lattice of Au NP as observed in Figure 3e−g mainly depends on the surface adsorption behavior of a stabilizing agent.[27,28] Chalcone possesses greater amphiphilicity because of the open ring structure in comparison to naringin and that in turn facilitates a better surface adsorption of chalcone. Thus, surface-adsorbed chalcone provides necessary colloidal stability and hence produces fine colloidal suspension (Figure 3a(F)) unlike to that of naringin (Figure 3a(B)). A better surface adsorption of a stabilizing agent on the surface of growing nucleating center passivates different crystal planes and limits their participation in further crystal growth[22] that generates mainly spherical morphologies as shown in Figure 3e. In spherical morphologies, all crystal planes of the nucleating center participate almost equally in the growth process as evident from the X-ray diffraction (XRD) patterns of fcc crystal structure shown in the inset of Figure 3g. The peaks at 38.1°, 44.4°, 64.5°, 77.5°, and 81.2° are indexed as {111}, {200}, {200}, {311}, and {222} facets, respectively, and are consistent with fcc geometry of Au bulk. However, most of the NPs are merged with one another which might have triggered mainly due to strong hydrogen bonding existing between different hydroxyl groups of surface-adsorbed chalcone molecules that may lead to interparticle fusion of growing nucleating centres.[20]

Ag and Pd NPs Synthesis. Naringin is unable to reduce the Ag^+ into Ag^0 in acidic medium (Figure 4a(A)), while the reduction is low at neutral pH (Figure 4a(B)) but significantly facilitated in basic medium (Figure 4a(C)). Here too, the chalcone form possesses stronger reduction potential to convert Ag^+ into Ag^0 in comparison to naringin as observed previously for the Au NPs. Extraction of the Ag NPs from "bottle C" into the organic phase can be done by using IL as shown in the sequence of "D → E" that produces a clear characteristic absorbance due to SPR around 420 nm (Figure 4b). TEM images of samples prepared at pH 7 and 11.5 are shown in Figure 4c,d and e,f, respectively. The former sample produces mainly long needles of crystallized naringin with embedded Ag NPs while the latter sample produces mainly monodisperse small Ag NPs. A low-resolution TEM image of naringin microneedles is shown in Figure S3, while a magnified image of a section of needle is shown in Figure 4c. Ag NPs can be seen as black dots embedded on the surface of microneedles. Its high-resolution image clearly shows the embedded crystalline Ag NP of ∼16 nm (Figure 4d). Ag NPs produced in basic medium are spherical and highly monodisperse of ≤20 nm (Figure 4e,f), and their corresponding XRD patterns depicting the fcc crystal structure are shown

DOI: 10.1021/acsomega.8b01776
ACS Omega 2018, 3, 15606−15614

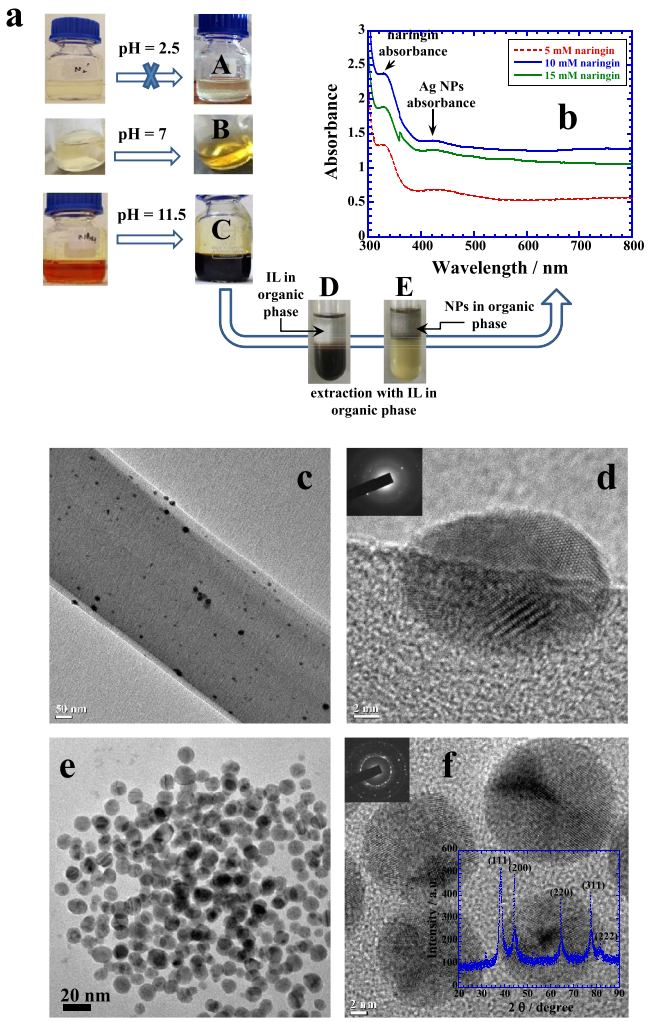

Figure 4. (a) Reaction sequences of in situ reaction of naringin with 0.25 mM of aqueous $AgNO_3$, at pH = 2.5, 7, and 11.5. Bottles "A", "B", and "C" show the Ag NP solutions prepared, respectively. No reaction occurs at pH 2.5. Solution "C" can be extracted into the organic phase, and (b) its corresponding UV−visible spectra with different concentrations of naringin. Panels (c,d) show the TEM images of self-crystallized naringin along with entrapped Au NPs prepared at pH 7, while (e,f) images of monodispersed Ag NPs prepared by using its chalcone at pH 11.5. Inset of (f) depicts the XRD patterns of Ag NPs. See details in text.

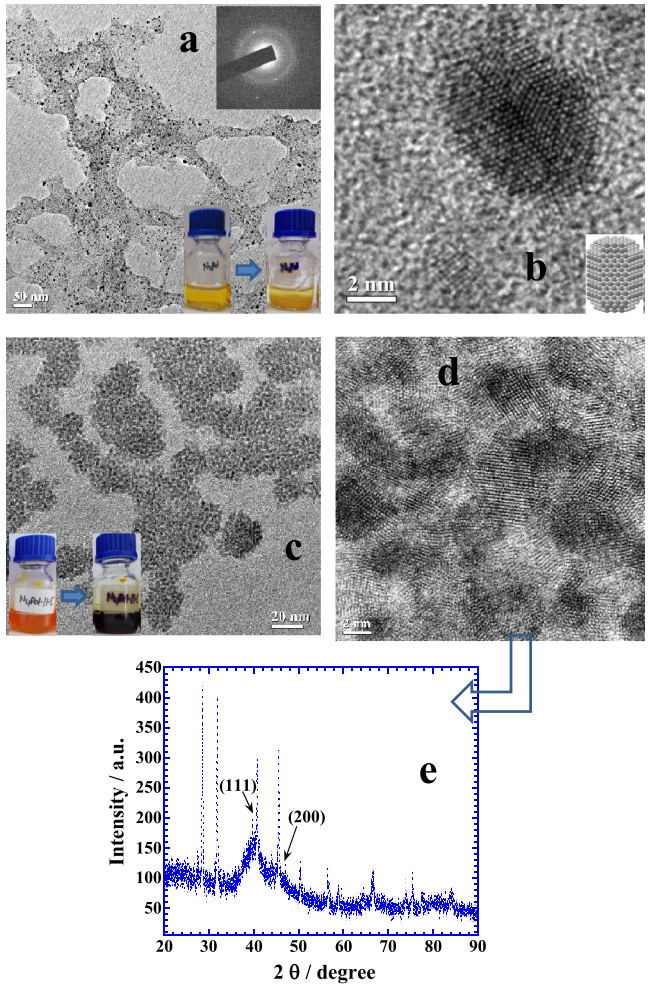

Figure 5. (a,b) TEM images of self-crystallized naringin along with entrapped Pd NPs prepared at pH 7 with 0.25 mM of aqueous K_2PdCl_4, while (c,d) images of self-assembled Pd NPs entrapped in its chalcone prepared at pH 11.5. (e) XRD patterns of Pd NPs. See details in text.

in the inset of Figure 4f. All peaks[29] show almost equal and prominent crystal growth spread over all crystal planes of fcc geometry leading to spherical monodisperse morphologies demonstrating fine shape control effect of chalcone.

Similarly, both naringin and its chalcone produce fine Pd NPs but naringin also crystallizes in large flakes (Figure S4) at neutral pH that produces a dark yellow suspension (see the yellow color of the bottle before and after the reaction in the inset of Figure 5a) while entrapping tiny Pd NPs of ≤5 nm (Figure 5a). A high-resolution image of single Pd NP shows that it is bound with mainly {110} crystal planes (Figure 5b). When the same reaction is conducted in basic medium, the reaction is quite facilitated by chalcone and produces flowerlike assemblies[30−32] of small Pd NPs (Figure 5c). The high-resolution image (Figure 5d) shows that groups of crystalline NPs of less than ∼4 nm are self-assembled in flowerlike arrangement which is usually induced by the interparticle interactions driven by the surface adsorbed chalcone. XRD patterns of this sample (Figure 5e) show only two weak diffraction peaks at 40.1° and 46.6°, while other two peaks at 68.1° and 82.2° of Pd fcc geometry are not visible. These peaks can be assigned to the {111}, {200}, {220}, and {311} crystal planes of fcc crystalline Pd.[32] Rest of the peaks belong to crystallized flavonoid and were not visible in the XRD patterns of Figures 3g and 4f for Au and Ag NPs, respectively, suggesting a much greater amount of both naringin and chalcone adsorbed on Pd NPs rather than on Au or Ag NPs. The origin of this is related to the noble nature of Au and Ag while the Pd nanosurface is highly reactive and encourages the adsorption and rearrangement of other molecules[33,34] in terms of its catalytic behavior that promotes the excessive adsorption of flavonoids.

Surface Adsorption of Naringin. The surface adsorption of naringin has been further evaluated by titrating presynthesized citrate and cetyltrimethylammonium bromide (CTAB)-stabilized Au/Ag/Pd seeds (see the Experimental Section) with naringin and simultaneously measuring UV−visible, dynamic light scattering (DLS), and zeta potential. Figure 6a,b depicts the UV−visible profiles of titration of naringin with citrate and CTAB-stabilized Au seeds. Free naringin

DOI: 10.1021/acsomega.8b01776
ACS Omega 2018, 3, 15606−15614

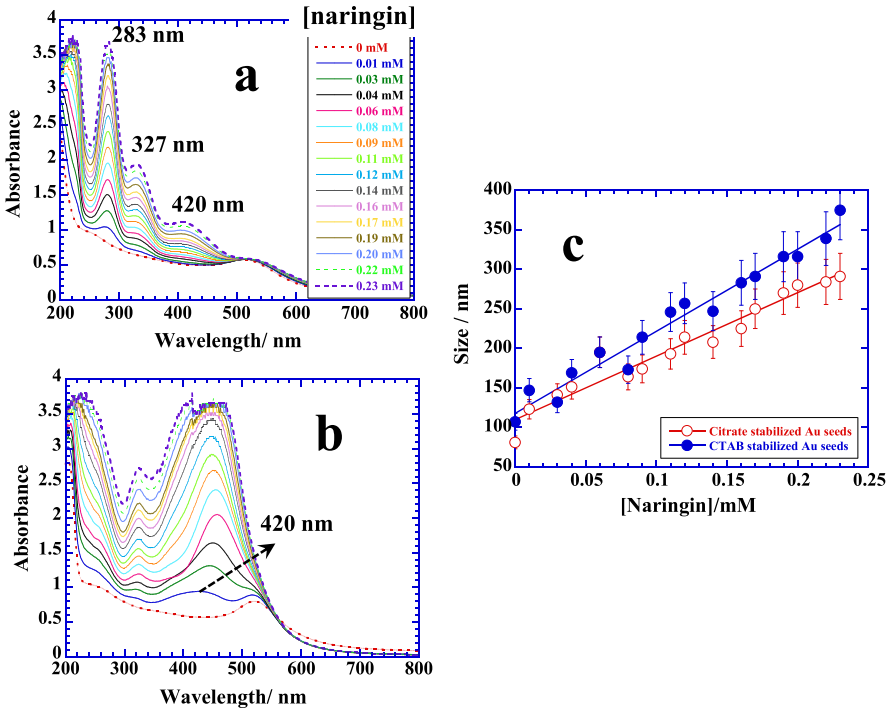

Figure 6. (a,b) UV−visible scans of titration of naringin with citrate-stabilized and CTAB-stabilized Au seeds, respectively, at 70 °C. (c) plots of corresponding DLS titrations depicting the size variation with respect to the concentration of naringin. See details in text.

demonstrates two main absorptions at 283 nm corresponding to ring "1" and another relatively weaker one at 327 nm due to ring "3" (see Figure 1),[35] while a weak broad band that emerges at 420 nm is due to the adsorption of naringin on the citrate-stabilized seeds. The latter peak becomes highly prominent and red-shifts with a dramatic increase in its intensity when instead of citrate, CTAB-stabilized Au seeds are used (Figure 6b). It also eliminates the absorption at 283 nm, suggesting the fact that the adsorption of naringin on CTAB-stabilized seeds is primarily induced by the ring "1" portion of naringin. DLS measurements (hydrodynamic diameter) further supplement this information. Stronger adsorption on CTAB-stabilized seeds leads to a continuous increase in the size with a greater slope in comparison to that on the citrate-stabilized seeds, which is considered to be weaker and driven by the hydrogen bonding[36,37] between the hydroxyl groups of naringin and tricarboxylic groups of citrate. Stronger electrostatic interactions operate between electronegative naringin due to the presence of several hydroxyl groups as well as ether oxygens and cationic CTAB-stabilized seeds. CTAB-stabilized seeds are always covered with a surfactant bilayer, where cationic head groups are aqueous solubilized. This arrangement allows cationic head groups to undergo electrostatic interactions with naringin molecules. A similar behavior is observed for the adsorption of naringin on citrate and CTAB-stabilized Ag seeds (Figure S5a), but no clear difference of naringin adsorption on citrate or CTAB-stabilized Pd seeds can be made most probably due to the highly active nature of Pd surface (Figure S5b).

Zeta potential measurements provide a better insight in the mechanism of adsorption of naringin on charged NP surface, and the results are presented in Figure 7. Figure 7a shows that the positive potential of CTAB-stabilized Au seeds converts to negative potential upon a complete deposition and passivation of the NPs surfaces by 0.08 mM naringin which is ∼3 mole ratio of CTAB-stabilized Au seeds/naringin. A similar behavior of zeta potential of CTAB-stabilized Ag and Pd seeds is observed upon the addition of naringin (Figure 7b,c) with mole ratios 3 and 4, respectively. It clearly shows that the deposition of naringin on positively charged CTAB-stabilized Au/Ag/Pd seeds is driven by the electrostatic interactions between the cationic ammonium head groups of CTAB and electronegative ether oxygens of naringin. However, surface adsorption of naringin of citrate-stabilized Au/Ag/Pd seeds seems to be quite different from the CTAB-stabilized seeds. It occurs instantaneously and rapidly on citrate-stabilized Ag and Pd seeds, prompting the change of negative zeta potential to zero within the same concentration range as it happens on CTAB-stabilized seeds (Figure 7b,c, respectively). A change of negative zeta potential to zero suggests the replacement of citrate by naringin on Ag/Pd surfaces that eventually provides the negative zeta potential due to the presence of electron rich hydroxyl and ether oxygens of naringin. In contrast, negative zeta potential of citrate-stabilized Au seeds never reaches to zero and remains almost unchanged up to the addition of 0.15 mM naringin but increases thereafter and eventually merges with the profile of CTAB-stabilized Au seeds around 0.2 mM naringin (Figure 7a). The origin of this behavior is related to the adsorption strength of citrate ions on different metallic surfaces. Citrate ions are excellent colloidal stabilizer for nano-Au seeds in comparison to Ag or Pd of similar shape and size. Citrate-stabilized Au seeds are stable for several weeks because of the strong adsorption of citrate ions on Au surface.[19,22] Naringin molecules are unable to replace the strongly adsorbed citrate ions rather prefer to interact through hydrogen bonding that allows the Au seeds to retain their negative zeta potential. This surface adsorption behavior of naringin on different nanometallic surfaces proves to be the determinant in protein extraction in the next section.

DOI: 10.1021/acsomega.8b01776
ACS Omega 2018, 3, 15606−15614

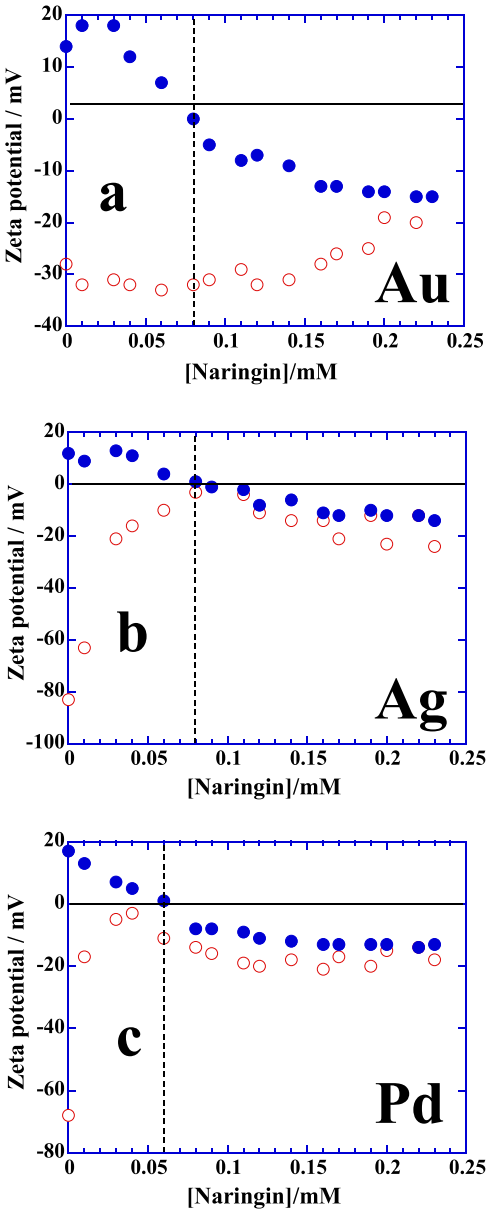

Figure 7. (a–c) Zeta potential titrations of citrate (empty diamonds) and CTAB (filled diamonds)-stabilized Au, Ag, and Pd seeds with naringin, respectively. See details in text.

Protein Extraction and Characterization. Flavonoids are also known for their interactions with proteins, and hence, Au/Ag/Pd NPs synthesized under in situ reaction conditions at pH 7 (Figures 3–5, respectively) are used for the extraction of protein fractions from zein corn starch protein aqueous suspension. Zein is highly important and versatile protein[23,38,39] because of its wide applicability in the food industry. Extraction ability of purified NPs samples is demonstrated by using the SDS page analysis as mentioned in the Experimental Section, and the results are presented Figure 8. Pure zein provides bands of 21.3, 25.7, 45.7, and 66 kDa of four different fractions.[23] The first two bands indicate the presence of α-zein,[38,39] while the next two bands are due to dimerization or oligomerization.[40] Unfolding of zein is related to the amount of SDS used and low amounts of SDS, that is, in the low mM concentration range greater than its critical micelle concentration partially reduce zein.[41] Partially reduced

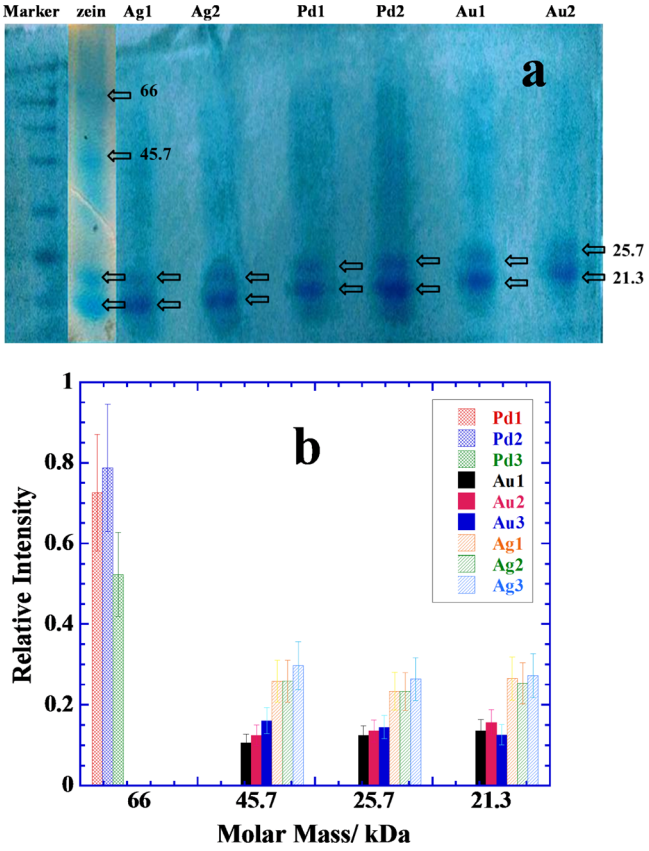

Figure 8. (a) Typical SDS page analysis scans of extracted zein protein fractions picked by the samples of naringin-conjugated NPs prepared with 0.25 mM metal salts and different concentrations of naringin (5 mM = 1, 10 mM = 2, and 15 mM = 3). See NPs images in Figures 3–5. (b) Comparative bar plots of relative amounts of the most abundant proteins picked by different samples. See details in the text.

zein is prone to oligomerization due to seeding[42] which is usually more prominent in the case of water insoluble proteins because of the presence of large proportions of nonpolar amino acids. Figure 8a shows that some typical SDS page scans for different NPs and the extraction of different zein fractions are NPs specific. Quantitative interpretation is depicted in Figure 8b, where extraction ability of a specific NP sample in terms of relative band intensity of SDS page analysis is plotted for each fraction.

Pd NPs mainly pick the protein fraction of 66 kDa, while Au/Ag NPs pick almost all in relatively lower amounts except the zein fraction of 66 kDa (Figure 8b). These preferences are primarily related to the amount of naringin adsorbed and deposited on each kind of NP surface during the in situ reaction conditions as well as nature of the metallic surfaces. Pd NPs exist in highly aggregated state with a large amount of naringin deposited on their surfaces (Figure 5). Therefore, an excessive amount of naringin coating is probably driving the protein extraction, while there is no possibility of protein fraction to directly adsorb on the naked Pd NP surface. Thus, the surface adsorption of smaller fractions which usually prefer naked metallic surfaces[43−45] is unable to adsorb allowing only the bigger fraction of 66 kDa to be extracted preferentially. This is due to the fact that the smaller protein fractions are usually less hydrophobic in comparison to bigger ones. Oligomeric fractions (such as that of 66 kDa) attain greater

DOI: 10.1021/acsomega.8b01776
ACS Omega 2018, 3, 15606−15614

nonpolarity due to the charge neutralization or hydrogen bonding. Similarly, several layers of adsorbed naringin on Pd NPs surface also attain greater nonpolarity due to the hydrogen bonding that exists among naringin molecules and hence prefers to extract zein fraction of 66 kDa rather than smaller fractions. This is not the case for Au and Ag NPs, where no excessive amount of naringin is visible in Figures 3 and 4, respectively, and hence, the protein extraction is driven both by the surface adsorbed naringin as well as naked Au/Ag surfaces. Both Au and Ag NPs show almost equal preference for all zein fractions except that for 66 kDa, while Ag NPs extract greater amount of each fraction in comparison to that extracted by the Au NPs. Self-crystallization of naringin in large needles (Figures 3 and 4) allows relatively much less amount of naringin adsorbed on Au and Ag NPs surface, thereby allowing naked NP surface an ideal choice for the smaller zein fractions to adsorb.

Concluding Remarks. The present results conclude that both naringin and its chalcone form can be used for the in situ synthesis of flavonoid conjugated nanomaterials, but chalcone is much more effective in reducing the metallic ions into nanometallic state, controlling the crystal growth and producing stable colloidal suspensions of Au, Ag, and Pd NPs. These NPs can be easily transferred to organic phase by using the water-insoluble IL for their appropriate applications in organic phase. The Au and Ag NPs are fairly monodisperse with a size close to 15 nm, whereas Pd NPs are less than 5 nm. Among them, the Pd NP surface attracts excessive deposition of both naringin as well as chalcone that leads to the self-aggregation of Pd NPs. The mechanism of NP surface adsorption of naringin is studied by using the citrate and CTAB-stabilized presynthesized Au, Ag, and Pd seeds. DLS and zeta potential measurements show that surface adsorption of naringin is highly facilitated and closely controlled by both electrostatic interactions as well as hydrogen bonding.

Naringin-conjugated NPs demonstrated their excellent potential in protein fractions extraction from aqueous zein suspension and that is clearly controlled by the amount of naringin deposition on nanometallic surfaces. Pd NPs with excessive deposition of naringin preferentially extract bigger or oligomeric zein fraction, whereas both Au and Ag NPs with much less amount of naringin adsorption only extract zein fractions of smaller molar masses. These results highlight the potential uses of naringin-conjugated NPs for their biotechnological applications with clear distinction between the low and high molar masses of protein fractions.

EXPERIMENTAL SECTION

Materials. Naringin from citrate fruit, chloroauric acid ($HAuCl_4$), silver nitrate ($AgNO_3$), potassium tetrachloropalladate (K_2PdCl_4), CTAB, sodium borohydride ($NaBH_4$), and citric acid trisodium salt (Na_3Cit) were purchased from Aldrich. Double-distilled water was used for all preparations. Extra care was taken to protect the aqueous solution of $HAuCl_4$ and $AgNO_3$ from light. Both solutions were used as freshly prepared and kept in the dark. Aqueous solutions of $NaBH_4$ and Na_3Cit were always used as freshly prepared.

METHODS

Naringin−Chalcone-Mediated Synthesis of Au, Ag, and Pd NPs. Both naringin and its chalcone form were used for the in situ synthesis of different nanomaterials without using any external reducing or stabilizing agent. For a typical reaction in acidic, neutral, or basic media, aqueous solutions of 5−40 mM naringin and 0.25 mM respective metal salts ($HAuCl_4$, $AgNO_3$, or K_2PdCl_4) were taken in screw-capped glass bottles and kept in a water thermostat bath (JULABO F25) at precise 70 ± 0.1 °C for 6 h under static conditions in the dark to protect against photoreduction. After 6 h, the samples were cooled to room temperature and kept for overnight. Each sample produced either settled or suspended NPs suspensions, which were purified with pure water at least three times. Purification was done by collecting the NPs at 8000−10 000 rpm for 5 min after washing each time with distilled water.

Flavonoid Complexation with Presynthesized NPs. Presynthesized Au, Ag, and Pd NPs (seeds) were produced by mixing $[HAuCl_4]/[AgNO_3]/[K_2PdCl_4]$ = 0.5 mM and $[Na_3Cit]$ = 0.5 mM, followed by the addition of 0.6 mL of ice cold aqueous $NaBH_4$ ($[NaBH_4]$ = 0.1 mol dm^{-3}) solution under constant stirring.[19,20] This reaction produced citrate-stabilized polyhedral Au/Ag/Pd seeds and are the best models to compare the adsorption of naringin on NP surfaces with those produced above under in situ reaction conditions. It was done by taking calculated amounts of presynthesized seeds in small UV−visible cuvettes and then titrated with freshly prepared aqueous naringin. Similar titrations were performed with DLS and zeta potential measurements to determine the change in the size and polarity of the seeds.

CHARACTERIZATION

Spectroscopic Analysis. Some of the reactions were simultaneously monitored with the help of UV−visible (Shimadzu—model no. 2450, double beam) and steady state fluorescence spectroscopy (PTI QuantaMaster) measurements. Both instruments were equipped with a TCC 240A thermoelectrically temperature-controlled cell holder that allowed the measurement of the spectrum at a constant temperature within ±1 °C.

Microscopy. All NP samples were characterized by TEM analysis on a JEOL 2010F system at an operating voltage of 200 kV. The samples were prepared by mounting a drop of a solution on a carbon coated Cu grid and allowed to dry in the air. DLS and zeta potential measurements were performed using a light scattering apparatus (Zetasizer Nano series, Nano-ZS, Malvern Instruments) equipped with a built-in temperature controller with an accuracy of ±0.1 °C. The measurements were made using a quartz cuvette with a path length of 1 cm. An average of 5 measurements was analyzed using the standard algorithms with an uncertainty of less than 7%. Aqueous suspension of each sample is placed in the cuvette to determine the size and zeta potential. Size distribution histogram was constructed by using the software provided with the instrument.

The XRD patterns were characterized by using a Bruker-AXS D8-GADDS system with T_{sec} = 480. Samples were prepared on glass slides by spotting a concentrated drop of aqueous suspension and were then dried in a vacuum desiccator.

SDS Page Gel Electrophoresis. SDS page was used for the characterization of zein protein fractions selectively extracted by the flavonoid-conjugated NPs. Before the analysis, each purified sample was assorted with 1× sample loading buffer and boiled in a water bath at 100 °C to digest and dislodge the protein complexed with naringin-protected

DOI: 10.1021/acsomega.8b01776
ACS Omega 2018, 3, 15606−15614

nanomaterials. The suspension thus obtained was subjected to SDS page analysis. The sample (10 μL) was loaded in the well of 5% stacking gel which was solidified over 12% separating gel. The loaded gel was immersed with 1× Tris-glycine SDS gel running buffer and was electrophoresed at 120 V and 10 mA. The gel was stained and destained to obtain the clear visible bands.

■ ASSOCIATED CONTENT

Supporting Information

The Supporting Information is available free of charge on the ACS Publications website at DOI: 10.1021/acsomega.8b01776.

UV−visible titration plot of HCl to naringin solution; TEM images showing self-crystallization of naringin during the in situ reaction; and DLS plots of citrate-stabilized and CTAB-stabilized seeds with naringin (PDF)

■ AUTHOR INFORMATION

Corresponding Authors

*E-mail: bakshim@uwgb.edu (M.S.B.).
*E-mail: virgo16sep2005@gmail.com (P.K.).

ORCID

Mandeep Singh Bakshi: 0000-0003-1251-9590

Notes

The authors declare no competing financial interest.

■ ACKNOWLEDGMENTS

These studies were partially supported by the financial assistance from UWGB, NAS, Green Bay, and DST under nanomission research project [ref no. SR/NM/NS-1057/2015(G)], New Delhi. Dr. Gurinder Kaur thankfully acknowledges the financial support provided by the Research and Development Council (RDC) of Newfoundland and Labrador, NSERC, and the Office of Applied Research at CNA. P.K. acknowledges the TEM studies done by SAIF Lab, Nehu, Shillong.

■ REFERENCES

(1) Albach, R. F.; Redman, G. H.; Cruse, R. R. Annual and Seasonal Changes in Naringin Concentration of Ruby Red Grapefruit Juice. *J. Agric. Food Chem.* **1981**, *29*, 808−811.

(2) Gorinstein, S.; Leontowicz, H.; Leontowicz, M.; Krzeminski, R.; Gralak, M.; Delgado-Licon, E.; Martinez Ayala, A. L.; Katrich, E.; Trakhtenberg, S. Changes in Plasma Lipid and Antioxidant Activity in Rats As a Result of Naringin and Red Grapefruit Supplementation. *J. Agric. Food Chem.* **2005**, *53*, 3223−3228.

(3) Benavente-García, O.; Castillo, J. Update on Uses and Properties of Citrus Flavonoids: New Findings in Anticancer, Cardiovascular, and Anti-Inflammatory Activity. *J. Agric. Food Chem.* **2008**, *56*, 6185−6205.

(4) Ban, C.; Park, S. J.; Lim, S.; Choi, S. J.; Choi, Y. J. Improving Flavonoid Bioaccessibility Using an Edible Oil-Based Lipid Nanoparticle for Oral Delivery. *J. Agric. Food Chem.* **2015**, *63*, 5266−5272.

(5) Rao, K.; Imran, M.; Jabri, T.; Ali, I.; Perveen, S.; Shafiullah; Ahmed, S.; Shah, M. R. Gum Tragacanth Stabilized Green Gold Nanoparticles As Cargos for Naringin Loading: A Morphological Investigation Through AFM. *Carbohydr. Polym.* **2017**, *174*, 243−252.

(6) Feng, T.; Wang, K.; Liu, F.; Ye, R.; Zhu, X.; Zhuang, H.; Xu, Z. Structural characterization and bioavailability of ternary nanoparticles consisting of amylose, α-linoleic acid and β-lactoglobulin complexed with naringin. *Int. J. Biol. Macromol.* **2017**, *99*, 365−374.

(7) Zhuang, C.; Zhang, W.; Sheng, C.; Zhang, W.; Xing, C.; Miao, Z. Chalcone: A Privileged Structure in Medicinal Chemistry. *Chem. Rev.* **2017**, *117*, 7762−7810.

(8) Rosa, G. P.; Seca, A. M. L.; do Carmo Barreto, M.; Pinto, D. C. G. A. Chalcone: A Valuable Scaffold Upgrading by Green Methods. *ACS Sustainable Chem. Eng.* **2017**, *5*, 7467−7480.

(9) Wu, J.; Li, J.; Cai, Y.; Pan, Y.; Ye, F.; Zhang, Y.; Zhao, Y.; Yang, S.; Li, X.; Liang, G. Evaluation and Discovery of Novel Synthetic Chalcone Derivatives As Anti-Inflammatory Agents. *J. Med. Chem.* **2011**, *54*, 8110−8123.

(10) Montenegro, M. A.; Nazareno, M. A.; Borsarelli, C. D. Kinetic Study of the Photosensitized Oxygenation of the Flavanone Naringin and Its Chalcone. *J. Photochem. Photobiol., A* **2007**, *186*, 47−56.

(11) González, E. A.; Nazareno, M. A.; Borsarelli, C. D. Enthalpy-entropy compensation effect in the chalcone formation from naringin in water-ethanol mixtures. *J. Chem. Soc., Perkin Trans. 2* **2002**, *2*, 2052−2056.

(12) Satterfield, M.; Brodbelt, J. S. Enhanced Detection of Flavonoids by Metal Complexation and Electrospray Ionization Mass Spectrometry. *Anal. Chem.* **2000**, *72*, 5898−5906.

(13) Zhang, J.; Brodbelt, J. S. Silver Complexation and Tandem Mass Spectrometry for Differentiation of Isomeric Flavonoid Diglycosides. *Anal. Chem.* **2005**, *77*, 1761−1770.

(14) Yu, J.; Wang, L.; Walzem, R. L.; Miller, E. G.; Pike, L. M.; Patil, B. S. Antioxidant Activity of Citrus Limonoids, Flavonoids, and Coumarins. *J. Agric. Food Chem.* **2005**, *53*, 2009−2014.

(15) Cejudo Bastante, M. J.; Durán Guerrero, E.; Castro Mejías, R.; Natera Marín, R.; Rodríguez Dodero, M. C.; Barroso, C. G. Study of the Polyphenolic Composition and Antioxidant Activity of New Sherry Vinegar-Derived Products by Maceration With Fruits. *J. Agric. Food Chem.* **2010**, *58*, 11814−11820.

(16) Rolo-Naranjo, A.; Codorniu-Hernández, E.; Ferro, N. Quantum Chemical Associations Ligand−Residue: Their Role to Predict Flavonoid Binding Sites in Proteins. *J. Chem. Inf. Model.* **2010**, *50*, 924−933.

(17) Yokoyama, T.; Kosaka, Y.; Mizuguchi, M. Structural Insight into the Interactions Between Death-Associated Protein Kinase 1 and Natural Flavonoids. *J. Med. Chem.* **2015**, *58*, 7400−7408.

(18) Arts, M. J. T. J.; Haenen, G. R. M. M.; Wilms, L. C.; Beetstra, S. A. J. N.; Heijnen, C. G. M.; Voss, H.-P.; Bast, A. Interactions Between Flavonoids and Proteins: Effect on the Total Antioxidant Capacity. *J. Agric. Food Chem.* **2002**, *50*, 1184−1187.

(19) Bakshi, M. S. A Simple Method of Superlattice Formation: Step-by-Step Evaluation of Crystal Growth of Gold Nanoparticles through Seed−Growth Method. *Langmuir* **2009**, *25*, 12697−12705.

(20) Bakshi, M. S.; Possmayer, F.; Petersen, N. O. Aqueous-Phase Room-Temperature Synthesis of Gold Nanoribbons: Soft Template Effect of a Gemini Surfactant. *J. Phys. Chem. C* **2008**, *112*, 8259−8265.

(21) González, E. A.; Nazareno, M. A.; Borsarelli, C. D. Enthalpy-Entropy Compensation Effect in the Chalcone Formation From Naringin in Water-Ethanol Mixtures. *J. Chem. Soc., Perkin Trans. 2* **2002**, 2052−2056.

(22) Bakshi, M. S. How Surfactants Control Crystal Growth of Nanomaterials. *Cryst. Growth Des.* **2016**, *16*, 1104−1133.

(23) Aggarwal, R.; Khullar, P.; Mandial, D.; Mahal, A.; Ahluwalia, G. K.; Bakshi, M. S. Bipyridinium and Imidazolium Ionic Liquids for Nanomaterials Synthesis: PH Effect, Phase Transfer Behavior, and Protein Extraction. *ACS Sustainable Chem. Eng.* **2017**, *5*, 7859−7870.

(24) Tang, N.; Yan, W. Solubilities of Naringin Dihydrochalcone in Pure Solvents and Mixed Solvents at Different Temperatures. *J. Chem. Eng. Data* **2016**, *61*, 4085−4089.

(25) Liu, B.; Zhu, X.; Zeng, J.; Zhao, J. Preparation and physicochemical characterization of the supramolecular inclusion complex of naringin dihydrochalcone and hydroxypropyl-β-cyclodextrin. *Food Res. Int.* **2013**, *54*, 691−696.

(26) Martin-Benlloch, X.; Elhabiri, M.; Lanfranchi, D. A.; Davioud-Charvet, E. A Practical and Economical High-Yielding, Six-Step

DOI: 10.1021/acsomega.8b01776
ACS Omega 2018, 3, 15606−15614

Sequence Synthesis of a Flavone: Application to the Multigram-Scale Synthesis of Ladanein. *Org. Process Res. Dev.* **2014**, *18*, 613−617.
(27) Sathishkumar, P.; Gu, F. L.; Zhan, Q.; Palvannan, T.; Mohd Yusoff, A. R. Flavonoids mediated "Green" nanomaterials: A novel nanomedicine system to treat various diseases - Current trends and future perspective. *Mater. Lett.* **2018**, *210*, 26−30.
(28) Terenteva, E. A.; Apyari, V. V.; Dmitrienko, S. G.; Zolotov, Y. A. Formation of Plasmonic Silver Nanoparticles by Flavonoid Reduction: A Comparative Study and Application for Determination of These Substances. *Spectrochim. Acta, Part A* **2015**, *151*, 89−95.
(29) Bakshi, M. S. Room Temperature Surfactant Assisted Crystal Growth of Silver Nanoparticles to Nanoribbons. *J. Nanosci. Nanotechnol.* **2010**, *10*, 1757−1765.
(30) Ren, M.; Zou, L.; Yuan, T.; Huang, Q.; Zou, Z.; Li, X.; Yang, H. Novel Palladium Flower-Like Nanostructured Networks for Electrocatalytic Oxidation of Formic Acid. *J. Power Sources* **2014**, *267*, 527−532.
(31) Gu, Z.; Xiong, Z.; Ren, F.; Li, S.; Xu, H.; Yan, B.; Du, Y. Flower-Like PdCu Catalyst With High Electrocatalytic Properties for Ethylene Glycol Oxidation. *J. Taiwan Inst. Chem. Eng.* **2018**, *83*, 32−39.
(32) Bakshi, M. S. 1D Flower-Like Morphologies of Palladium Nanoparticles Using Strongly Hydrophobic Surfactants. *J. Phys. Chem. C* **2009**, *113*, 10921−10928.
(33) Long, R.; Mao, K.; Ye, X.; Yan, W.; Huang, Y.; Wang, J.; Fu, Y.; Wang, X.; Wu, X.; Xie, Y.; Xiong, Y. Surface Facet of Palladium Nanocrystals: A Key Parameter to the Activation of Molecular Oxygen for Organic Catalysis and Cancer Treatment. *J. Am. Chem. Soc.* **2013**, *135*, 3200−3207.
(34) Moreno, M.; Ibañez, F. J.; Jasinski, J. B.; Zamborini, F. P. Hydrogen Reactivity of Palladium Nanoparticles Coated With Mixed Monolayers of Alkyl Thiols and Alkyl Amines for Sensing and Catalysis Applications. *J. Am. Chem. Soc.* **2011**, *133*, 4389−4397.
(35) Zhang, L.; Song, L.; Zhang, P.; Liu, T.; Zhou, L.; Yang, G.; Lin, R.; Zhang, J. Solubilities of Naringin and Naringenin in Different Solvents and Dissociation Constants of Naringenin. *J. Chem. Eng. Data* **2015**, *60*, 932−940.
(36) Zhang, X.; Li, L.; Xu, Z.; Su, J.; Li, B.; Huang, J. Studies on the Interaction of Naringin Palmitate With Lysozyme by Spectroscopic Analysis. *J. Funct. Foods* **2014**, *8*, 331−339.
(37) Jung, D.-M.; de Ropp, J. S.; Ebeler, S. E. Study of Interactions between Food Phenolics and Aromatic Flavors Using One- and Two-Dimensional1H NMR Spectroscopy. *J. Agric. Food Chem.* **2000**, *48*, 407−412.
(38) Zhu, F.; Kale, A. V.; Cheryan, M. Fractionation of Zein by Size Exclusion Chromatography. *J. Agric. Food Chem.* **2007**, *55*, 3843−3849.
(39) Esen, A. A proposed nomenclature for the alcohol-soluble proteins (zeins) of maize (Zea mays L.). *J. Cereal Sci.* **1987**, *5*, 117−128.
(40) Paulis, J. W. Disulfide Structures of Zein Proteins from Corn Endosperm. *Cereal Chem.* **1981**, *58*, 542−546.
(41) Mahal, A.; Khullar, P.; Kumar, H.; Kaur, G.; Singh, N.; Jelokhani-Niaraki, M.; Bakshi, M. S. Green Chemistry of Zein Protein Toward the Synthesis of Bioconjugated Nanoparticles: Understanding Unfolding, Fusogenic Behavior, and Hemolysis. *ACS Sustainable Chem. Eng.* **2013**, *1*, 627−639.
(42) Bakshi, M. S. Nanoshape Control Tendency of Phospholipids and Proteins: Protein-Nanoparticle Composites, Seeding, Self-Aggregation, and Their Applications in Bionanotechnology and Nanotoxicology. *J. Phys. Chem. C* **2011**, *115*, 13947−13960.
(43) Bakshi, M. S.; Kaur, H.; Banipal, T. S.; Singh, N.; Kaur, G. Biomineralization of Gold Nanoparticles by Lysozyme and Cytochrome c and Their Applications in Protein Film Formation. *Langmuir* **2010**, *26*, 13535−13544.
(44) Manikas, A. C.; Causa, F.; Della Moglie, R.; Netti, P. A. Tuning Gold Nanoparticles Interfaces by Specific Peptide Interaction for Surface Enhanced Raman Spectroscopy (SERS) and Separation Applications. *ACS Appl. Mater. Interfaces* **2013**, *5*, 7915−7922.
(45) Oishi, J.; Asami, Y.; Mori, T.; Kang, J.-H.; Niidome, T.; Katayama, Y. Colorimetric Enzymatic Activity Assay Based on Noncrosslinking Aggregation of Gold Nanoparticles Induced by Adsorption of Substrate Peptides. *Biomacromolecules* **2008**, *9*, 2301−2308.

DOI: 10.1021/acsomega.8b01776
ACS Omega 2018, 3, 15606−15614